Effect of an elastic wall on the behavior of encapsulated microbubbles

L. Aired, A. A. Doinikov and A. Bouakaz

INSERM U930 CNRS ERL3106, Université François Rabelais, CHU Bretonneau, 2 Blvd.
Tonnellé, 37044 Tours, France
leila.aired@etu.univ-tours.fr

The aim of this work is to study how boundaries with different mechanical properties affect the acoustic response of contrast agent microbubbles. To this end, numerical simulations are performed for two types of walls: a polystyrene (OptiCell) wall and a biological tissue. For each wall, the behavior of contrast microbubbles of three sizes is investigated. The spectral characteristics of the scattered pressure produced by the microbubbles are compared for two cases: the bubble oscillates far away from the wall and the same bubble oscillates in the immediate vicinity of the wall. The results of the simulations allow one to draw the following main conclusions. The effect of the OptiCell wall on the acoustic bubble response is stronger than that of the tissue wall. Changes in the bubble response near the wall are stronger when bubbles are excited above their fundamental resonance frequency. Changes are stronger for smaller bubbles and changes in the 2nd harmonic are stronger than those in the fundamental. The results obtained allow one to gain an insight into conditions under which the effect of an elastic wall on the acoustic response of a contrast agent microbubble is easier to be detected.

1   Introduction

Much work has been done on the investigation of the effect of a confining surface on the dynamics of a free (unencapsulated) bubble, mainly in the context of the problem of cavitation damage. In clinical applications, such as targeted ultrasound imaging [1,2], the boundary is the wall of a blood vessel. In experiments, contrast microbubbles interact with the walls of experimental containers which can be made of different materials [3-5]. Experimental data show that the proximity of a boundary can produce considerable changes in the oscillation amplitude of a contrast agent microbubble and its scattered echo [3-6]. Available theoretical studies predict that the resonance frequency of a contrast microbubble near a boundary can either decrease or increase depending on the mechanical properties of the boundary [7-10]. However, these effects still remain little-studied.

The purpose of the present study is to reveal how boundaries with different mechanical properties affect the acoustic response of a contrast agent microbubble. To this end, the following research is carried out. We conduct numerical simulations for two boundaries whose parameters correspond to the mechanical properties of an OptiCell wall and a biological tissue. The simulations are based on a theory that has been developed recently in [9,10]. In these papers, a modified Rayleigh-Plesset equation was derived that describes the radial oscillation of a contrast agent microbubble near an elastic wall of finite thickness. We use this equation to model the oscillation of contrast microbubbles of different size near the two types of walls mentioned above. Then we use these data to calculate the scattered echoes from the microbubbles when they oscillate near the different walls. Finally, we compare these echoes with those produced by the same microbubbles when they are far away from the walls. The ultimate goal of this work is to establish the conditions of excitation that make it possible to distinguish the scattered echoes generated by the microbubbles near and far away from the walls.

2   Model

The equation derived in [9,10] for a contrast microbubble pulsating near an elastic wall of finite thickness is given by

$$R\ddot{R}\left[1-\left(\frac{\rho_1-\beta}{\rho_1+\beta}\right)\frac{R}{2d}-\left(\frac{\beta-\rho_3}{\beta+\rho_3}\right)\frac{R}{2(d+h)}+\frac{(\rho_1-\beta)(\beta-\rho_3)}{(\rho_1+\beta)(\beta+\rho_3)}\frac{R}{2h}\right]$$

$$+\frac{3}{2}\dot{R}^2\left[1-\left(\frac{\rho_1-\beta}{\rho_1+\beta}\right)\frac{2R}{3d}-\left(\frac{\beta-\rho_3}{\beta+\rho_3}\right)\frac{2R}{3(d+h)}+\frac{(\rho_1-\beta)(\beta-\rho_3)}{(\rho_1+\beta)(\beta+\rho_3)}\frac{2R}{3h}\right]$$

$$=\frac{1}{\rho_1}\left[\left(P_0+\frac{2\sigma}{R_0}\right)\left(\frac{R_0}{R}\right)^{3\gamma}-\frac{2\sigma}{R}-4\eta\frac{\dot{R}}{R}-P_0-P_{ac}(t)-S\right], (1)$$

where $R(t)$ is the instantaneous radius of the bubble, the overdot denotes the time derivative so that $\dot{R}=dR/dt$ and $\ddot{R}=d^2R/dt^2$, ρ_1 is the density of the liquid surrounding the bubble, d is the distance between the bubble center and the wall, ρ_3 is the density of the liquid behind the wall, h is the thickness of the wall, P_0 is the hydrostatic pressure in the liquid surrounding the bubble, σ is the surface tension, R_0 is the bubble radius at rest, γ is the ratio of specific heats of the gas inside the bubble, η is the shear viscosity of the liquid, $P_{ac}(t)$ is the driving acoustic pressure, and the term S describes the effect of encapsulation.

The parameter β in (1) characterizes the mechanical properties of the wall and is defined as

$$\beta=\rho_2\frac{3\mathrm{K}-2\mu}{3\mathrm{K}+4\mu}, \qquad (2)$$

where ρ_2, K, μ are the density, the bulk modulus, the shear modulus of the wall, respectively.

If the term S in (1) is specified by the de Jong shell model [11,12], (1) takes the form:

$$R\ddot{R}\left[1-\left(\frac{\rho_1-\beta}{\rho_1+\beta}\right)\frac{R}{2d}-\left(\frac{\beta-\rho_3}{\beta+\rho_3}\right)\frac{R}{2(d+h)}+\frac{(\rho_1-\beta)(\beta-\rho_3)}{(\rho_1+\beta)(\beta+\rho_3)}\frac{R}{2h}\right]$$

$$+\frac{3}{2}\dot{R}^2\left[1-\left(\frac{\rho_1-\beta}{\rho_1+\beta}\right)\frac{2R}{3d}-\left(\frac{\beta-\rho_3}{\beta+\rho_3}\right)\frac{2R}{3(d+h)}+\frac{(\rho_1-\beta)(\beta-\rho_3)}{(\rho_1+\beta)(\beta+\rho_3)}\frac{2R}{3h}\right]$$

$$=\frac{1}{\rho_1}\left[\left(P_0+\frac{2\sigma}{R_0}\right)\left(\frac{R_0}{R}\right)^{3\gamma}\left(1-\frac{3\gamma}{c}\dot{R}\right)-\frac{2\sigma}{R}-4\eta\frac{\dot{R}}{R}-P_0-P_{ac}(t)\right.$$

$$\left.-4\chi\left(\frac{1}{R_0}-\frac{1}{R}\right)-\frac{4\kappa_S\dot{R}}{R^2}\right], \qquad (3)$$

where c is the speed of sound in the liquid surrounding the bubble, κ_S is the shell viscosity, and χ is the shell elasticity [13].

It is also shown in [9,10] that the scattered pressure from the bubble in the far-field zone, i.e., at a distance much larger than the bubble size, is calculated as

$$p_{scat}=\frac{\rho_1(R^2\ddot{R}+2R\dot{R}^2)}{L}\frac{4\beta\rho_3}{(\rho_1+\beta)(\beta+\rho_3)}, \qquad (4)$$

where L denotes the distance between the center of the bubble and the point of measurement. It is assumed that L is large compared to d and h (see figure 1).
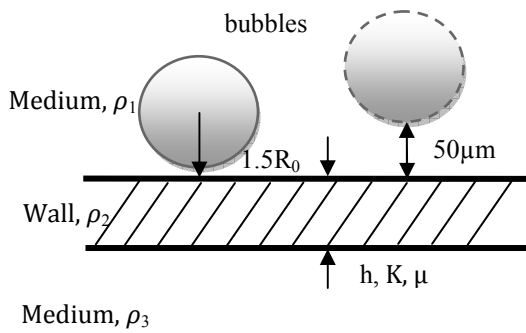

Figure 1: Two situations compared in the simulations.

It is well known that the shell parameters of contrast agents are dependent on bubble size. To take this effect into account, we use experimental data from [12] that show the dependence of the shell elasticity and the shell viscosity on bubble size in the case that experimental radius-time curves are fitted by the de Jong shell model.

3   Numerical simulations

The simulations have been carried out by means of the program MATHEMATICA (Wolfram Research, Inc., Champaign, IL). The values of the physical parameters used in (3) and (4) were set to be: $P_0 = 101.3$ kPa, $\rho_1 = \rho_3 = 1000$ kg/m^3, $\eta = 0.001$ Pa·s, $c = 1480$ m/s, $\sigma = 0.072$ N/m, $\gamma = 1.095$, and $L = 0.01$ m. The excitation is an 8-cycle, 200 kPa Gaussian pulse with a center frequency in the range $1-5$ MHz.

The two types of walls are tested in our simulations: a plastic wall and a biological tissue. The mechanical parameters of the walls were set to be: for the plastic wall, $\rho_2 = 1060$ kg/m^3, $K = 3.75$ GPa, $\mu = 1.34$ GPa; for tissue, $\rho_2 = 960$ kg/m^3, $K = 0.124$ GPa, $\mu = 0.0062$ GPa. The properties of the plastic wall were chosen to correspond to the walls of OptiCell chambers (Nunc, Fisher Scientific, France) which are commonly used in experiments [5,14,15]. The parameters for tissue were adopted from [16]. The thickness of both walls was taken to be equal to h = 75 µm. This value corresponds to the wall thickness of OptiCell chambers [14] and is on the same order as the wall thickness of arterial vessels [17,18].

The behavior of bubbles of three sizes is investigated: $R_0 = 1.5$, 2, and 3 µm. The values of the shell parameters for each bubble size are calculated by the interpolation of experimental points obtained in [12]. For each wall and for each bubble, two situations shown in figure 1 are compared: the bubble is in the immediate vicinity of the wall ($d = 1.5R_0$) and the same bubble is far away from the wall ($d = 50$ µm).
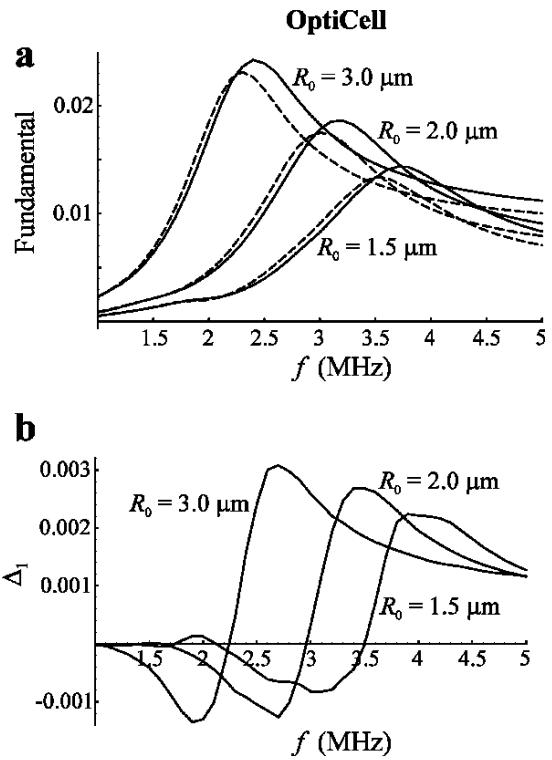

Figure 2: (a) The magnitude of the fundamental component in the spectrum of the bubble scattered pressure versus driving frequency for the OptiCell wall. The solid lines correspond to the bubbles at $d = 1.5R_0$ and the dashed lines to the same bubbles at $d = 50$ µm. (b) The deviation of the solid curves from the dashed curves.
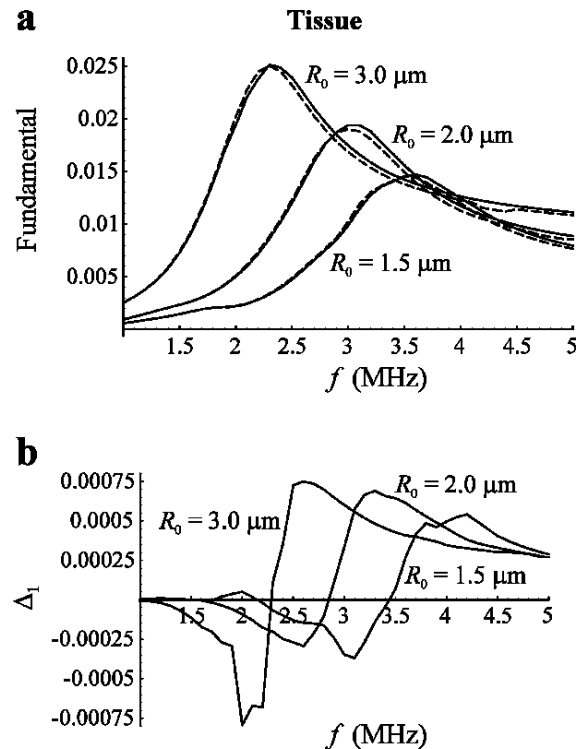

Figure 3: (a) The magnitude of the fundamental component in the spectrum of the bubble scattered pressure versus driving frequency for the tissue wall. The solid lines correspond to the bubbles at $d = 1.5R_0$ and the dashed lines to the same bubbles at $d = 50$ µm. (b) The deviation of the solid curves from the dashed curves.
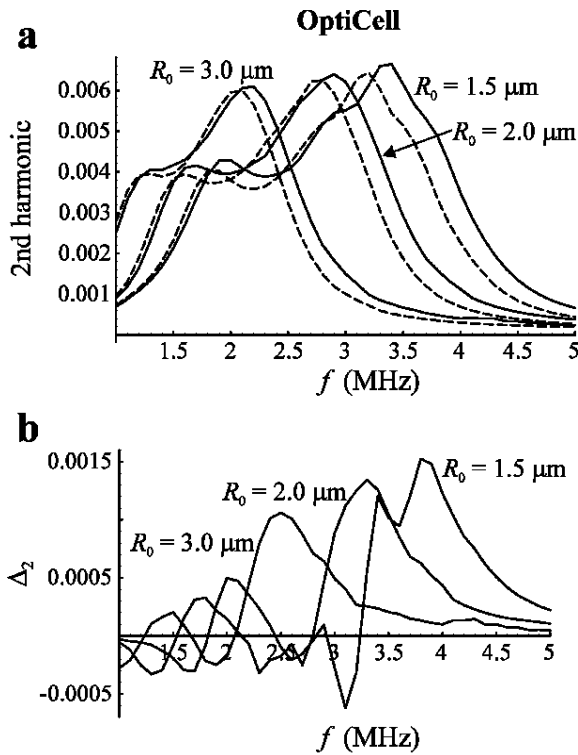
a OptiCell

b

Figure 4: (a) The magnitude of the 2nd harmonic component in the spectrum of the bubble scattered pressure versus driving frequency for the OptiCell wall. The solid lines correspond to the bubbles at $d = 1.5R_0$ and the dashed lines to the same bubbles at $d = 50$ μm. (b) The deviation of the solid curves from the dashed curves.
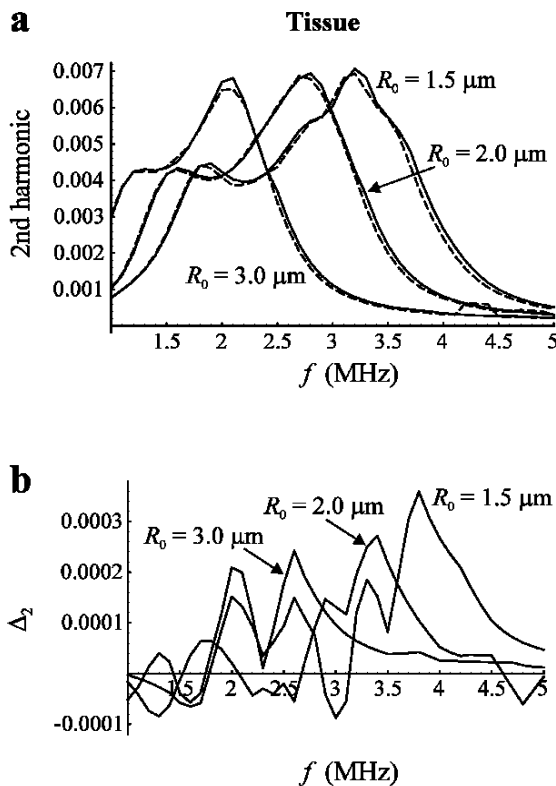
a Tissue

b

Figure 5: (a) The magnitude of the 2nd harmonic component in the spectrum of the bubble scattered pressure versus driving frequency for the tissue wall. The solid lines correspond to the bubbles at $d = 1.5R_0$ and the dashed lines to the same bubbles at $d = 50$ μm. (b) The deviation of the solid curves from the dashed curves.

Figure 2a shows the magnitude of the fundamental component in the spectrum of the bubble scattered pressure as a function of the driving frequency for the OptiCell wall. The solid lines correspond to the bubbles at $d = 1.5R_0$, and the dashed lines to the same bubbles at $d = 50$ μm. Note that all the curves are normalized by the acoustic pressure amplitude (200 kPa). For better visualization, the deviation of the solid curves from the dashed curves is shown in figure 2b. As one can see, the magnitude and the sign of the deviation depend on the value of the driving frequency. Figure 3 provide similar data for the tissue wall. The comparative analysis of figure 2 and 3 reveals that more considerable changes are observed for the OptiCell wall. One can see that the influence of the wall is stronger when the bubbles are excited slightly above resonance. It is also seen that for both walls, the difference between the solid and dashed curves is greater for the larger bubbles.

Figure 4 and 5 show the normalized magnitude of the 2nd harmonic in the spectrum of the scattered pressure as a function of the driving frequency for the same cases as in figures 2 and 3. The OptiCell wall is again in the lead. Notice that, in contrast to the fundamental, the 2nd harmonic is changed more strongly for the smaller bubbles.
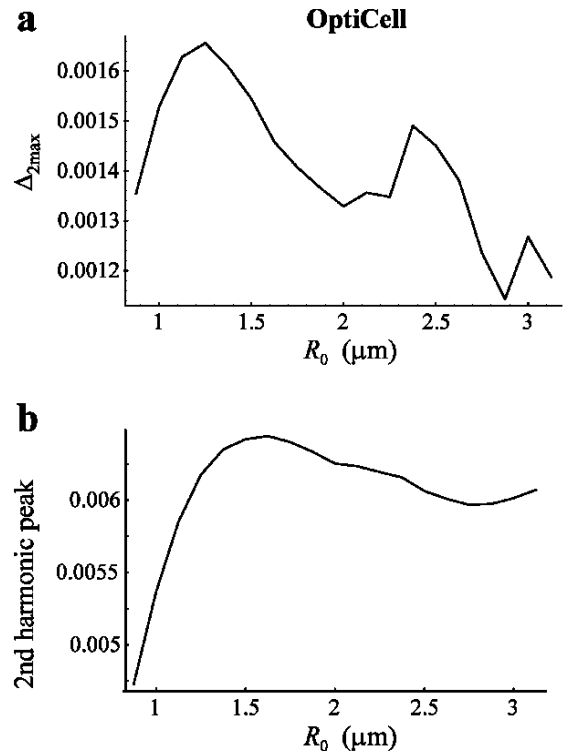
a OptiCell

b

Figure 6: (a) The maximum increase of the 2nd harmonic near the OptiCell wall as a function of equilibrium bubble radius. (b) The peak value of the 2nd harmonic versus bubble radius.

Figure 6 shows the maximum increase of the 2nd harmonic that is reached near OptiCell wall for each bubble size. The form of this curve is likely to be related to the nonmonotonic dependence of the peak value of the 2nd harmonic on bubble size (see figure 6b). One can see again that the proximity of the wall affects more strongly smaller bubbles.
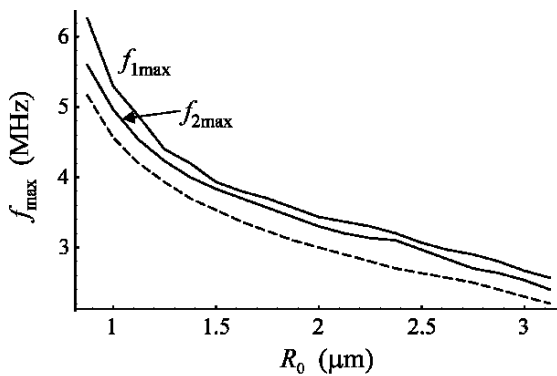
Figure 7: $f_{1\,max}$ and $f_{2\,max}$ are the driving frequencies at which the maximum increases of, respectively, the fundamental and the 2nd harmonic are reached at different bubble radii. The dashed line shows the fundamental resonance frequency of bubbles.

Finally, figure 7 shows the driving frequencies $f_{1\,max}$ and $f_{2\,max}$ at which the maximum increases of, respectively, the fundamental and the 2nd harmonic take place. The dashed line corresponds to the fundamental resonance frequency. It is seen that the maximum increase of both the fundamental and the 2nd harmonic is observed when the bubbles are driven above resonance.

4   Conclusion

In this study, the effect of confining surfaces with different mechanical properties on the acoustic response of a contrast agent microbubble has been investigated numerically. As a theoretical basis, the equations derived previously by the authors in [9,10] were used. These equations describe the radial oscillation of a contrast microbubble near an elastic wall of finite thickness and the scattered pressure produced by the microbubble in the far-field zone. The numerical simulations were made for two walls whose parameters corresponded to the mechanical properties of a plastic (OptiCell) wall and a biological tissue. For each wall, the behavior of bubbles of three sizes was investigated. The spectral characteristics of the scattered pressure produced by the bubbles were compared for two cases, namely, when the bubble oscillated far away from the wall and when the same bubble oscillated in the immediate vicinity of the wall. The results of our simulations allow one to make the following main conclusions. Near the OptiCell wall, more considerable changes in the bubble behavior occur than near the tissue. The influence of the OptiCell wall on the acoustic response of a contrast agent microbubble has the following features. Changes in both the fundamental and the 2nd harmonic near the wall are stronger when bubbles are excited above resonance. The difference between the magnitudes of the fundamental component near and far away from the wall is increased with increasing bubble size, whereas the same difference for the 2nd harmonic is greater in the range of bubble radii from about 1.0 to 1.6 μm. It was also found that the relative difference for the 2nd harmonic, i.e., the absolute difference divided by the peak value of the 2nd harmonic, is higher than that for the fundamental. The results obtained provide an insight into conditions under which the effect of an elastic wall on the acoustic response of a contrast agent microbubble is easier to be detected.

References

[1] S.H. Bloch, P.A. Dayton, K.W. Ferrara, "Targeted imaging using ultrasound contrast agents: Progress and opportunities for clinical and research applications", *IEEE Eng.Med. Biol. Mag.* 23, 18-29 (2004)

[2] A.L. Klibanov, "Microbubble contrast agents: Targeted ultrasound imaging and ultrasound-assisted drug-delivery applications", *Invest. Radiol.* 41, 354-362 (2006)

[3] S. Zhao, D.E Kruse, K.W. Dayton, "Asymmetric oscillation of adherent targeted ultrasound contrast agents", *Appl. Phys. Lett.* 87, 1341031-1341033 (2005)

[4] S. Zhao, D.E. Kruse, K.W. Ferrara, P.A. Dayton, "Acoustic response from adherent targeted contrast agents", *J. Acoust. Soc. Am.* 120, EL63–EL69 (2006)

[5] V. Garbin, D. Cojoc, E. Ferrari, E. Di Fabrizio, M.L.J. Overvelde, S.M. van der Meer, N. de Jong, D. Lohse, M. Versluis, "Changes in microbubble dynamics near a boundary revealed by combined optical micromanipulation and high-speed imaging", *Appl. Phys. Lett.* 90 114103 (2007).

[6] M. Lankford, C.Z. Behm, J. Yeh, A.L. Klibanov, P. Robinson, J.R. Lindner, "Effect of microbubble ligation to cells on ultrasound signal enhancement: implications for targeted imaging", *Invest. Radiol.* 41, 721–728 (2006)

[7] S. Qin, K.W. Ferrara, "The natural frequency of nonlinear oscillation of ultrasound contrast agents in microvessels", *Ultrasound Med. Biol.* 33, 1140–1148 (2007)

[8] S. Martynov, E. Stride, N. Saffari, "The natural frequencies of microbubble oscillation in elastic vessels", *J. Acoust. Soc. Am.* 126, 2963–2972 (2009)

[9] A.A. Doinikov, L. Aired, A. Bouakaz, "Modeling and experiments on the far-field scattering of a bubble pulsating near a wall with finite density and thickness", *Proceedings of the 2010 IEEE International Ultrasonics Symposium, IEEE, San Diego, California, USA*, 1133–1136 (2010)

[10] A.A. Doinikov, L. Aired, A. Bouakaz, "Acoustic scattering from a contrast agent microbubble near an elastic wall of finite thickness", *Phys. Med. Biol.* 56, 6951–6967 (2011).

[11] S.M. van der Meer, B. Dollet, M.M. Voormolen, C.T. Chin, A. Bouakaz, N. de Jong, M. Versluis, D. Lohse, "Microbubble spectroscopy of ultrasound contrast agents", *J. Acoust. Soc. Am.* 121, 648–656 (2007)

[12] J. Tu, J. Guan, Y. Qiu, T.J. Matula," Estimating the shell parameters of SonoVue® microbubbles using light scattering", *J. Acoust. Soc. Am.* 126, 2954–2962 (2009)

[13] P. Marmottant, S. van der Meer, M. Emmer, M. Versluis, N. de Jong, S. Hilgenfeldt, D. Lohse, "A model for large amplitude oscillations of coated bubbles accounting for buckling and rupture", *J. Acoust. Soc. Am.* 118, 3499–3505 (2005)

[14] V. Garbin, E. Ferrari, D. Cojoc, E. Di Fabrizio, M.L.J. Overvelde, S.M. van der Meer, M. Versluis, N. de Jong, D. Lohse, "Optical trapping of ultrasound

contrast agent microbubbles: study of the bubble-wall and bubble-bubble interaction in ultrasound", *Proceedings of the 2006 IEEE International Ultrasonics Symposium, IEEE, Vancouver, BC, Canada*, 513–516 (2006)

[15] M. Overvelde, V. Garbin, J. Sijl, B. Dollet, N. de Jong, D. Lohse, M. Versluis, "Nonlinear shell behavior of phospholipid-coated microbubbles", *Ultrasound Med. Biol*. 36, 2080–2092(2010).

[16] M. Bechel, G. Noble, R. Ratliff, R.T. Hart, "Fluid-Structure Interaction in a Network of Blood Vessels", http://www.comsol.com/showroom/gallery/660/, p. 5.

[17] D.H. Bergel, "The static elastic properties of the arterial wall", *J. Physiol*. 156, 445–457 (1961)

[18] D.H. Bergel, "The dynamic elastic properties of the arterial wall", *J. Physiol*. 156, 458–469 (1961)